Mass balance reconstruction for Shiyi Glacier in the Qilian Mountains, Northeastern Tibetan Plateau, and its climatic drivers

Hui Zhang[1,2] · Zhongqin Li[1,2] · Ping Zhou[1]

Abstract

Based on glacio-meteorological records, 7 years of in-situ mass balance data, and a temperature-index model, the long-term annual and seasonal mass balances of Shiyi Glacier in the northeast Tibetan Plateau (TP) were reconstructed from 1963/64 to 2016/17. Variations were then linked to local climatic and macroscale circulation changes. The model was calibrated based on in-situ mass balance data and was driven by daily air temperature and precipitation data recorded at nearby alpine meteorological stations. The results show that the reconstructed annual mass balance experienced an overall downward trend over the past 54 years, with a remarkably high mass loss rate during 1990/91–2016/17. Analysis of mass balance sensitivity and local climatic changes shows that the pronounced mass loss since the 1990s can be mainly attributed to cumulative positive temperature increases caused by air temperature increases and prolongation of the ablation season. From the perspective of macroscale circulation, the reconstructed annual mass balance values correlate well with zonal wind speeds (June to September) in the glacierized region. For the positive/negative phase of the annual mass balance, an inverse spatial pattern in relation to geopotential height change (low/high-pressure centres) and corresponding conversion of cyclonic/anti-cyclonic circulation were present in northern hemisphere mid-latitudes. Comparative analysis of existing long-term mass balance series over the TP indicates that asynchronous climatic changes in the different glacierized regions led to inconsistent interannual fluctuations in glacier mass balance.

1 Introduction

Glacier mass balance is one of the variables that is essential to climatic system monitoring (Zemp et al. 2009). It is widely adopted to explain the glacial ablation process and glacier-atmospheric interactions. Thus, glacier mass balance has broad relevance to regional hydrological modelling, water resource assessment and sea-level rise (Kaser et al. 2006; Cogley 2009; Fujita et al. 2011; Zemp et al. 2013; Marzeion et al. 2014). However, alpine glaciers often occur in inaccessible mountainous terrain, causing great difficulties for filed observation. Glacier mass balance observation obtained by glaciological method is more time-consuming and labour-intensive than other types of glaciological observations, making it difficult to conduct for long periods. For these reasons, there is little global-scale in-situ data (Zemp et al. 2019), particularly in the TP and similar mountainous regions. Among Tibetan glaciers, long-term mass balance observations are only available for the Xiaodongkemadi

✉ Hui Zhang
zhanghui@lzb.ac.cn

1 State Key Laboratory of Cryospheric Science, Northwest Institute of Eco-Environment and Resources, Tianshan Glaciological Station, Chinese Academy of Sciences (CAS), Lanzhou 730000, China

2 State Key Laboratory of Cryospheric Science, Northwest Institute of Eco-Environment and Resources, Altai Observation and Research Station of Cryospheric Science and Sustainable Development, Chinese Academy of Sciences (CAS), Lanzhou 730000, China

Glacier, which has been monitored since 1989. This lack of in-situ observations is the biggest limitation to dynamics simulation and forecasting (Yang et al. 2019). Therefore, there is an urgent need to fill mass balance observation gaps and extend data series in both the spatial and temporal scales.

The TP and surrounding mountains is the most highly glacierized region in the world apart from polar regions. It has a glacier area of 99,261 km^2, which forms the headwater region of the main large Asian rivers (Yao et al. 2012). Since the early 1980s, the TP has shown overall surface warming and moistening; its horizontal warming pattern is consistent with glacier recession (Yang et al. 2014). Affected by regional differences in climatic factors (such as air temperature, snowfall, net radiance, etc.), most glaciers in the TP and its surroundings have shrunk significantly since the 1960s, excluding the Karakorum Mountains, Western Kunlun Mountains, and eastern Pamir (Bolch 2012; Gardelle et al. 2013; Neckel et al. 2014; Kääb et al. 2015; Brun et al. 2017; De Kok et al. 2018; Bonekamp et al. 2019; Kumar et al. 2019; Farinotti et al. 2020; Shean et al. 2020). There is clear spatial heterogeneity in glacier shrinkage, which increases gradually from the TP interior to the Himalayas (Yao et al. 2012). As Tibetan glaciers are critical to regional hydrological cycles, ecology, economies and global climate systems, its evolution characteristics, spatial heterogeneity and corresponding climatic mechanisms have drawn increased attention in international academic communities (Immerzeel et al. 2010; Bolch 2012; Yao et al. 2012; Yang et al. 2013, 2016; Zhu et al. 2018a; Brun et al. 2019; Liang et al. 2019).

Among several key glacial parameters, glacier mass balance is the best indicator of glacier-climate interactions (Oerlemans 1994; Braithwaite and Zhang 2000; Vincent 2002; Huss et al. 2008). Over recent decades, continuous mass balance observations (> 3 years) have been carried out for 15 glaciers in the TP (Yao et al. 2012). Meanwhile, reconstruction of annual mass balances has been conducted for the Qiyi Glacier, Parlung No.94 Glacier, Muztag Ata No.15 Glacier and Xiaodongkemadi Glacier, based on mass balance models and meteorological data (Wang et al. 2010; Yang et al. 2016; Zhu et al. 2018b; Liang et al. 2019; Fig. 1). However, long-term mass balance data remain scarce, especially for Qilian Mountain. Therefore, a strategy that combines in-situ mass balance data and meteorological data in a suitable mass balance model to reconstruct the long-term glacier mass balance is essential to understanding climate-glacier processes and the spatiotemporal variability of Tibetan glaciers.

For the Hulugou Basin (HLB) where Shiyi Glacier is located, an integrated meteorological cryosphere-hydrology observation system was established in 2008. So far, observations and studies in glacier and meteorology have been conducted (Chen et al. 2014, 2015; Liu and chen 2016; Liu et al.

2016), which have provided a useful database for follow-up studies. This study aims to reconstruct the long-term mass balance series of Shiyi Glacier using a temperature-index model based on glacio-meteorological records and mass balance data. We then discuss its climatic drivers and relationship with macroscale circulations. The results will aid the interpretation of intra-regional variability in glacier mass balance and provide a basis for predicting water availability in the TP.

2 Study area

Shiyi Glacier (38.21° N, 99.88° E; Randolph Glacier Inventory ID: RGI60-13.31537) is located in the upstream area of the HLB in the middle section of the Qilian Mountains at the northeastern edge of the TP (Fig. 1). This glacier is the largest in the HLB. It covered an altitude range of 4320–4775 m a.s.l., a total surface extent of 0.44 km^2, and had a maximum thickness of 70 m in 2010 based on the field observation. Shiyi Glacier is a typical continental (cold-type) glacier (Shi 2008) and can be divided into two parts according to its morphological characteristics: a steep western branch with northerly exposure and a flat eastern branch with northeasterly exposure. During the past 55 years, its surface extent only decreased 15.6% (Chen et al. 2014) and the geodetic mass balance was -0.53 ± 0.11 m w.e.a^{-1} for the period 2000–2012 (Xu et al. 2019). According to observational data (2011–2012) from an automatic weather station (AWS) near the glacier terminus (38.22° N, 99.89° E; 4166 m), the mean annual temperature was -5.4 °C and the mean annual precipitation was 776.7 mm, of which ~ 29% fell as snow (Chen et al. 2015).

3 Data and methods

3.1 Meteorological data

This study used meteorological data (daily temperature and precipitation) from two meteorological observation points (P1 and P2) in the HLB, and a nearby national meteorological station (Yeniugou Meteorological Station; Fig. 1). The data of station P1 and station P2 were provided by the Qilian Alpine Ecology and Hydrology Research Station (Qilian station), Chinese Academy of Sciences. And the data of Yeniugou Meteorological Station (YNG) was acquired from the National Meteorological Information Center, China Meteorological Administration (available at https://data.cma.cn/). Station P1 (38.27° N, 99.88° E, 2980 m) is located at the basin outlet, and recorded daily precipitation by a Chinese standard precipitation gauge (CSPG) located in a pit from September 2010 to April 2015. For detailed instrument
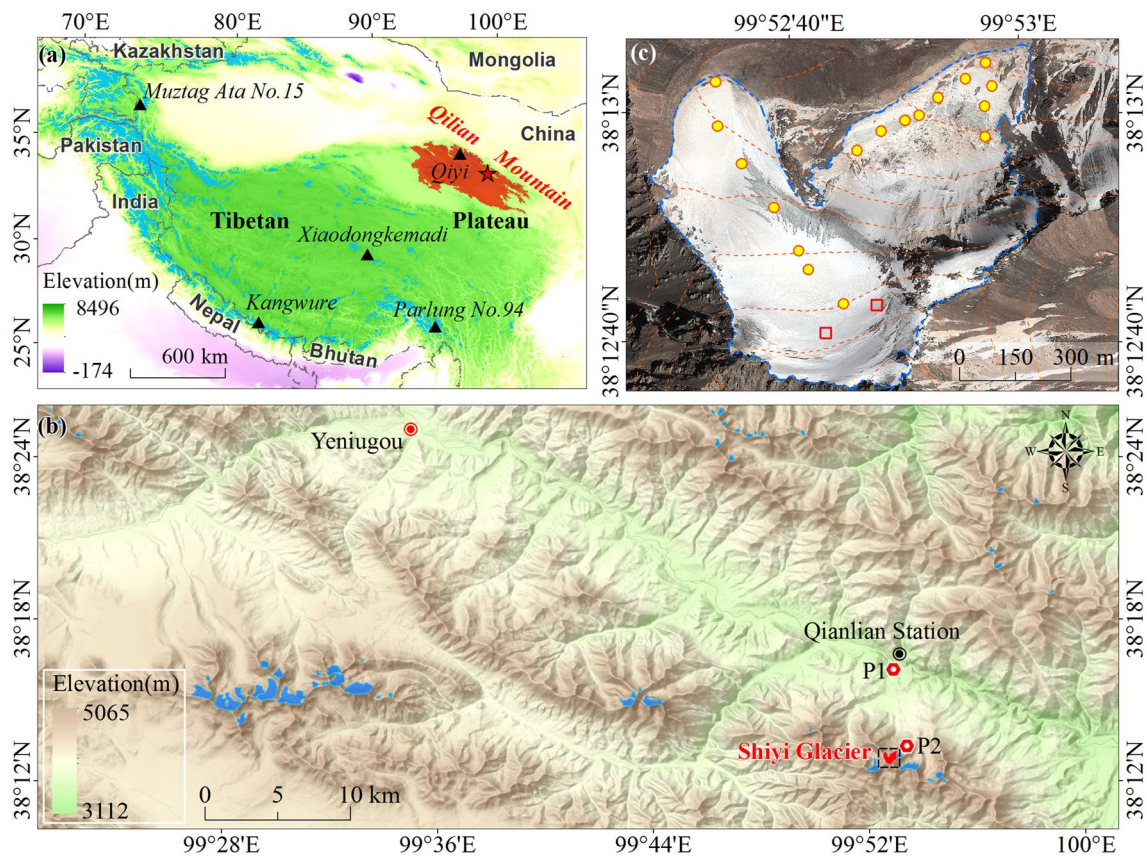
Fig. 1 Maps showing **a** the location of Shiyi Glacier (red star), the spatial extent of the Qilian Mountains (red zone), and the locations of five selected glaciers with long-term mass balance measurements (black triangles) on the TP; **b** the site of Qilian station (black circle) and distribution of Yeniugou meteorological stations (red circles) and two observation points (red hexagons) in the HLB based on a combination of coloured elevation and shaded-relief images derived from the Shuttle Radar Topography Mission digital elevation model (SRTM DEM); and **c** the locations of stakes (yellow circles) and snow pits (red squares) on the glacier surface in 2011 based on a Google Earth image acquired on 28 March 2013. The blue and red dotted lines indicate the boundary of Shiyi Glacier and the contour line of the glacierized region, and the black dotted rectangle indicates the spatial extent of map (**b**). Glaciers in maps **a** and **b** are marked by blue colour and Shiyi Glacier is marked by red colour in map (**b**). Glacier outlines were derived from the Randolph Glacier Inventory version 6

specifications, refer to Chen et al. (2015). Station P2 (38.22° N, 99.89° E, 4166 m) was only ~0.63 km away from the glacier terminus. It is an AWS that collected temperature and precipitation data from 1 December 2010 to 15 December 2013 [for detailed instrument specifications, refer to Chen et al. (2014, 2015) and Liu et al. (2016)]. The YNG station (38.42° N, 99.58° E, 3320 m) is the closest alpine meteorological station, located approximately 30 km away from the glacier terminus at a similar altitude. Temperature data from P2 and YNG are highly correlated ($r = 0.98$, $p < 0.01$). The daily precipitation series at different observation points (P1, P2 and YNG) are also correlated well in the corresponding period ($r = 0.73$ for YNG and P1; $r = 0.71$ for YNG and P2; $r = 0.78$ for P1 and P2, $p < 0.01$ in all cases). To generate a continuous meteorological dataset (1963–2017) for model forcing, we downscaled the daily temperatures from YNG station based on an empirical relationship, which was

determined by comparison with meteorological observations at P2 during the corresponding period (Fujita and Nuimura 2011; Yang et al. 2016; Zhang et al. 2018). See Figure. S1 for details of the downscaling.

Given the high spatial variability for monthly precipitation in HLB (Chen et al. 2014), the precipitation for YNG was corrected via the ratio method (Yang et al. 2013) on a monthly scale. The ratios of monthly precipitation between YNG, P1 and P2 were derived through a comparison of the total precipitation amounts. See Table S1 for details of the ratios. The precipitation at YNG was interpolated to the P1 location initially, and then interpolated to P2 based on the ratios. Figure 2 displays observed meteorological variables at station P2 and corrected meteorological variables at station YNG from 1 October 2010–15 October 2013 and their root mean square errors.

Moreover, monthly geopotential height/wind fields at the 300 hPa level were utilized to explore the potential relationship between macroscale atmospheric circulation and glacier mass change. These were provided by the National Center for Environmental Prediction-National Center for Atmospheric Research (NCEP/NCAR) following Mölg et al. (2014) and Zhu et al. (2018a). Monthly values of climate indexes, including the EA (East Atlantic), EP-NP (East Pacific-North Pacific), PDO (Pacific Decadal Oscillation), WP (West Pacific), EA-WR (East Atlantic-Western Russia), NAO (North Atlantic Oscillation), PNA (Pacific-North American Pattern) and NP (North Pacific) were obtained from the National Weather Service, Climate Prediction Centre (NOAA) and National Center for Atmospheric Research (NCAR).

3.2 Glacier mass balance and surface extent

Glacier mass balance measurements for Shiyi Glacier have been conducted each year since 2010 at the end of August or beginning of September using the traditional glaciological method (Paterson 1994). A glacier mass balance observation network, including metal stakes and snow pits, was used, as displayed in Fig. 1. 17–25 special metal stakes were drilled into the ice by a portable steam drill (Heucke) and snow pits were dug at the accumulation zone location in the seven mass balance observation years. A mass balance year is divided into summer (May–October) and winter (September–April) glaciological seasons. Mass balance values for each stake were obtained by stake reading and corresponding snow pit observations (including snow depth and density measurements for each snow layer) from year to year. Assuming an ice density of 0.9 g.cm^{-3}, the measured ablation values were converted into water equivalents (m w.e.), then the net mass balance of the entire glacier was derived through the contour-line method.

In the past 54 years, the surface extent of Shiyi Glacier only decreased by 0.1 km^2 (-0.3% a^{-1}; Chen et al. 2014), which mainly occurred after 2000. Hence, the glacier surface extent after 2000 was updated based on orthorectified and georeferenced Landsat images (May–September) with low cloud coverage taken in 2000, 2003, 2007, 2011, 2013 and 2016 with an uncertainty of 5% (Paul et al. 2013), which were provided by the United States Geological Survey (USGS, https://glovis.usgs.gov/). Historical topography (1: 50,000) in 1956 and glacier outlines (in 2011, 2013 and 2016) measured by hand-held GPS during the summer period were also used. The reliability of digitized glacier outlines derived from remote sensing images was validated by GPS-aided field mapping in the corresponding year. Besides, the SRTM DEM was used to extract the altitudinal attributes of the glacier surface.
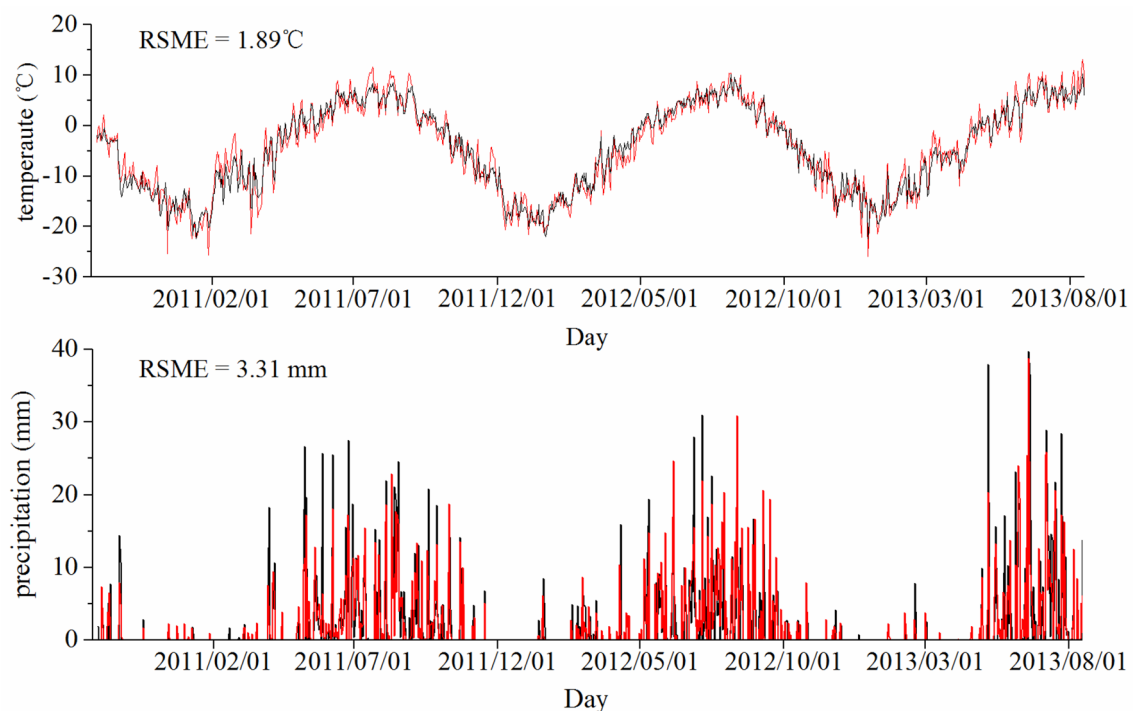
Fig. 2 Observed meteorological variables at station P2 (black lines) and corrected meteorological variables at station YNG (red lines) from 1 October 2010–15 October 2013

3.3 Glacier mass balance model

Temperature index models are commonly used to reconstruct the mass balance series (Kronenberg et al. 2016). They have been widely applied in a variety of glaciological studies (Braithwaite 1995; Braithwaite and Zhang 2000; Vincent 2002; Hock 2003; Pellicciotti et al. 2005; Zhang et al. 2006; Huss et al. 2008; Azam et al. 2014; Liu and Liu 2016; Barandun et al. 2018; Zhang et al. 2018) and perform better on mid-latitude glaciers (Sicart et al. 2008). In comparison with other melt models that include solar radiation, the temperature-index model is sufficient to model long-term glacier mass balance (Reveillet et al. 2017), especially when systematic meteorological observations on the glacier surface are limited. Therefore, we used the temperature-index model following Hock (2003), coupled with an accumulation model to calculate the annual and seasonal mass balances. The model relates the amount of ice/snow ablation with the positive degree-day sum by the separate degree-day factor. Accumulation is estimated based on the measured precipitation occurring at temperatures lower than a threshold temperature used for snow/rain separation.

The ablation M is calculated by

$$M = \begin{cases} DDF_{ice/snow}T_{air} & : T_{air} > 0 \\ 0 & : T_{air} \leq 0 \end{cases} \tag{1}$$

where $DDF_{ice/snow}$ indicates the degree-day factor (mm·day^{-1} °C) for ice/snow and T_{air} denotes the daily mean temperature (°C) at the respective glacier altitudes. In term of glacier surface type, we chose different degree-day factors separately for ice and snow surfaces.

The accumulation C is calculated by

$$C = \begin{cases} C_{prec}P & : T_{air} \leq T_P \\ 0 & : T_{air} > T_P \end{cases} \tag{2}$$

where P indicates the extrapolated precipitation (mm) at the respective glacier altitude and T_p denotes the threshold temperature (°C) for snow/rain separation. A scaling factor, C_{prec}, is used to adjust the precipitation totals and gauge measurement errors. Liquid precipitation and meltwater were assumed to flow away from the glacier instantly and refreezing was not considered (Machguth et al. 2012). The glacier surface was assumed to be bare ice at the beginning of the modelling periods. Temperature and precipitation measured at station P2 were used as model forcing data, which were interpolated to the corresponding altitude of the glacier surface. The model is based on a 90 m resolution DEM of the area; each glacier surface altitudinal range was defined as either bare ice or snow at the beginning of the modelling periods, and ice ablation was assumed to occur until the covered snow melted off. For a mass balance year, the mass balance was calculated at every altitudinal range

(50 m intervals) at a daily resolution using corresponding interpolated daily temperature and precipitation data.

Based on cryosphere-hydrology observations in the HLB, an average temperature lapse rate (TLR) of 0.48 °C (100 m)$^{-1}$, was determined by field measurements of air temperature from July 2009 to September 2011 (Chen et al. 2014; Liu and Chen 2016). According to basin-scale precipitation type observations in the HLB, the threshold temperature for discriminating rain-snow (T_p) at a daily resolution was found to be 0 °C.

The average DDF_{ice} and DDF_{snow} for Shiyi Glacier were also obtained from field experiments on the glacier surface during the ablation period (14–27 July 2011; 27 July–18 Oct 2012) (Fang et al. 2015). Assuming the precipitation at P2 was somewhat lower than that at the altitude of the glacier, the initial value for C_{pre} was set as 1.1 following Kronenberg et al. (2016). The precipitation gradient (δ_p/δ_z) was constrained by the available snow depth observations on the glacier surface (May 2011, July 2012 and June 2016), which ranged from 118.9–166.2 mm (100 m)$^{-1}$. The initial precipitation gradient (δ_p/δ_z) was set as the average.

3.4 Model calibration and uncertainty analysis

Model parameters (DDF_{ice}, DDF_{snow}, T_p, TLR) were adopted from field observations, which were assigned as constant over time. Considering the large spatial variability in accumulation on glacier surfaces due to complex topography, the C_{prec} and δ_p/δ_z values for each altitudinal range were varied until the resulting root mean square error (RMSE) between the measured and modelled values was minimised (following Azam et al. 2014). This resulted in a mean δ_p/δ_z of 136.8 mm (100 m)$^{-1}$. In addition to ensuring the robustness of the model parameters, C_{prec} was adjusted again until the average modelled mass balance matched the corresponding value determined geodetically from 2000 to 2012 following Huss et al. (2008). Then, the calibrated set of parameters (Table 1) was used to calculate the mass balance for the other years in the simulation period. The modelled and measured mass balances are compared in Fig. 3. The results indicate that the modelled and measured mass balances are in good agreement, with a Nash–Sutcliffe efficiency (NSE)

Table 1 Model parameters used for mass balance modelling

Melt-model parameter	Value	Unit
DDF_{ice}	6.3	mm day^{-1} °C
DDF_{snow}	4.5	mm day^{-1} °C
T_p	0	°C
TLR	0.48	°C (100 m)$^{-1}$
C_{prec}	1.4	–
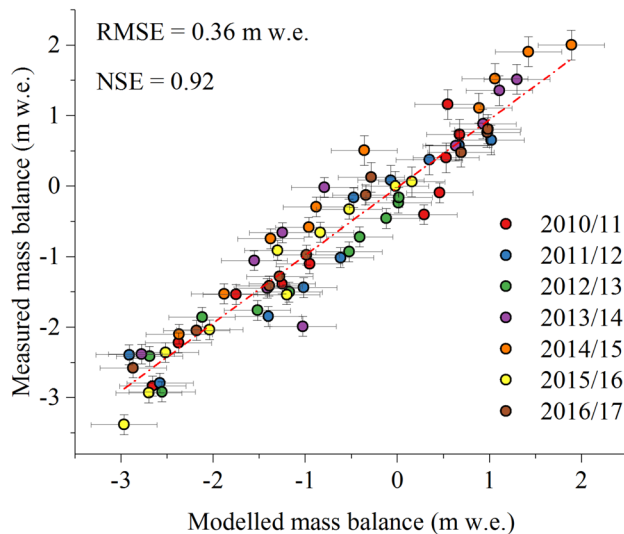
Fig. 3 Comparison of measured and modelled mass balance for each altitudinal range from 2010/11 to 2016/17

of 0.92 and RMSE of 0.36 m w.e.a^{-1}, which substantiates the model's performance.

The uncertainty in glaciological mass balance depends on the uncertainties in in-situ measurements of ablation and accumulation and the extrapolation of point measurements to the entire glacier area. Uncertainties in point measurements of ablation and accumulation were adopted from Thibert et al. (2008). The overall uncertainty (σ_{abl}) in annual point ablation measurements was estimated as $0.14/\sqrt{N}$ m w.e.a^{-1}, with an ice density of 0.9 g.cm^{-3} and N ablation measurements per year. Combining the uncertainties in density and snow depth measurements, the annual uncertainty in accumulation (excluding stratigraphic error) is $\sigma_{acc} = 0.21$ m w.e.a^{-1}. The uncertainties in extrapolation for the ablation area ($\sigma_{extr-abl}$) and accumulation in the area ($\sigma_{extr-acc}$) were obtained from Kenzhebaev et al. (2017). Combining the above uncertainties at different altitudinal ranges (Azam et al. 2012), the uncertainty in glaciological mass balance (σ_{glac}) was found to be 0.28 m w.e.a^{-1}.

Uncertainty (σ_{mod}) in modelled annual mass balance mainly originates from the parameter selection. To quantify the uncertainty, model parameters (DDF_{ice}, DDF_{snow}, C_{prec}, σ_p/σ_z and TLR) were adjusted by $\pm 25\%$ (Azam et al. 2014; Barandun et al. 2018; Zhu et al. 2018a) and the model was rerun. The standard deviation between the new modelled mass balance and corresponding initial value was adopted as an estimate of σ_{mod}. In our experiment, we found $\sigma_{mod} = 0.38$ m w.e.a^{-1}.

To estimate the model uncertainties due to missing parameter optimization for the periods 1963/64–1999/2000 and 2012/13–2016/17, we reran the model with average

values of the calibrated parameters (C_{prec} and σ_p/σ_z) following the method developed by Barandun et al. (2015). The standard deviation (σ_{opt}) between the optimized and non-optimized modelled mass balance results was used to interpret the uncertainties for periods without direct field measurements. We found that $\sigma_{opt} = 0.25$ m w.e.a^{-1}.

The uncertainty from unchanged glacier hypsometry was also evaluated following Azam et al. (2014), which revealed an uncertainty of $\sigma_{hyp} = 0.08$ m w.e.a^{-1}. As revealed by other studies (Azam et al. 2014; Barandun et al. 2015; Kenzhebaev et al. 2017), the uncertainty due to non-changed glacier surface elevations was lower. Additionally, considering the shrinkage of Shiyi Glacier over the simulation period, the glacier area in different elevation bands was updated yearly through the linear area interpolation method developed by Zemp et al. (2013) based on historical topography, Landsat images and in-situ measurements. The uncertainty in the calculation of glacier surface area for each altitudinal range was found to be 5% (Azam et al. 2012). Combined with the above uncertainty components, the overall uncertainty in modelled annual mass balance was estimated as ± 0.46 m w.e.a^{-1} by applying Gaussian error propagation.

4 Results

4.1 Reconstructed mass balance over the past 54 mass balance years

Mass balances for the Shiyi Glacier from 1963/64 to 2016/17 were reconstructed based on the calibrated model and corrected meteorological data. Figure 4 depicts the reconstructed annual mass balances together with measured net mass balances for the seven mass balance years. As shown, the reconstructed annual mass balance experienced an overall downward trend over the 54 mass balance years ($p < 0.01$ via linear regression), with a remarkably negative mass balance since the 1990s. The annual mass balance is characterized by high interannual variability, with a maximum of 1.23 m w.e. (in 1983/84) and a minimum of -1.55 m w.e. (in 1980/81). The cumulative mass balance was found to be -12.84 m w.e. over the 54 mass balance years, with an average of -0.24 m w.e.a^{-1}. According to the nonparametric Mann–Kendall test, the most likely abrupt change point occurred in 1989/90, which was verified by moving t-tests and the Yamamoto index (Yamamoto et al. 1986). Hence, two distinct phases were distinguished in the mass balance series, taking 1989/90 as the abrupt change point (Fig. 4). A positive phase (Phase I) occurred during the period 1963/64–1989/90, in which the annual mass balances are mainly positive and exhibit a slight upward trend ($p < 0.03$ via linear regression). Phase II (significant negative phase) occurred during the period 1990/91–2016/17. Only
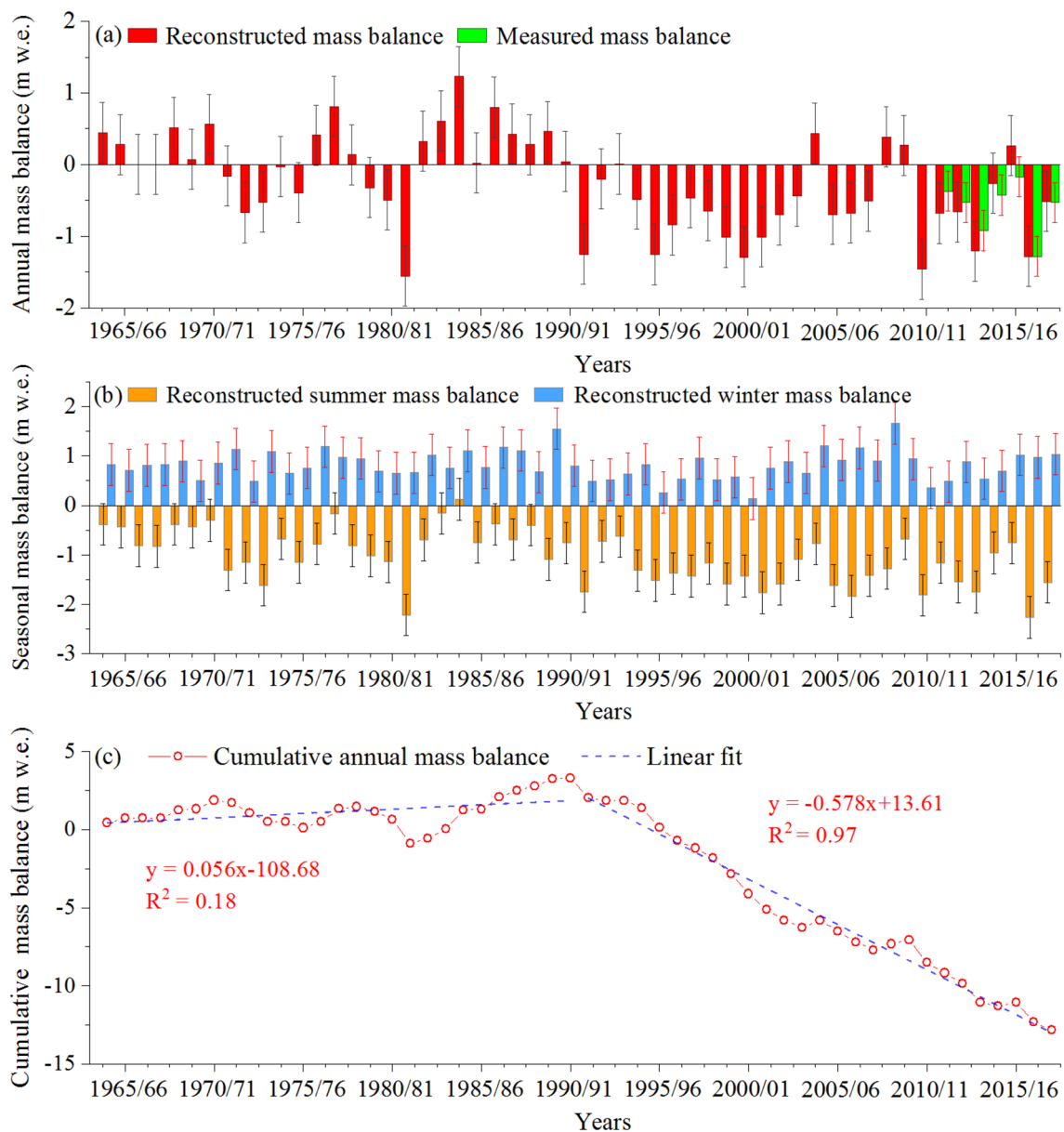
Fig. 4 Comparison between the measured and modelled annual mass balances (**a**), seasonal balances (**b**), and cumulative annual mass balances (**c**) of Shiyi Glacier during the period 1963/64–2016/17

four positive values appear among this phase and the annual mass balances show a remarkable downward trend overall ($p < 0.01$ via linear regression). The annual mass balance differed significantly between the two phases, with means of 0.12 m w.e.a^{-1} and -0.6 m w.e.a^{-1}, respectively. Overall, the mass balance of Shiyi Glacier showed a remarkable downward trend after 1989/90, resulting in mass loss concentrated in the period 1990/91–2016/17. Additionally, the simulation results show that the glacier had no accumulation zone in 2009/10 and 2012/13.

To further analyse the intra-annual variation in mass balance, seasonal mass balances were also reconstructed and

are displayed in Fig. 4. Reconstructed summer balances from 1963/64 to 2016/17 show large interannual variations and exhibit an obvious downtrend ($p < 0.01$ via linear regression). Over the 54 mass balance years, the summer balances are all negative except for 1983/84, and their interannual fluctuation is highly consistent with the annual balance. The mean summer mass balance in phase II (-1.36 m w.e.a^{-1}) is nearly twice that in phase I (-0.75 m w.e.a^{-1}), which indicates that the glacier mass loss rate in the summer period increased significantly after 1989/90. By comparison, the reconstructed winter balances over the 54 mass balance years exhibit low interannual variation with a slight overall

downward trend. The mean winter mass balance for phase I (0.88 m w.e.a^{-1}) is slightly larger than that of phase II (0.76 m w.e.a^{-1}); therefore, no significant periodic change exists. For the reconstructed monthly mass balances, overall decreasing trends were found for June ($p < 0.01$ via linear regression), July ($p < 0.01$ via linear regression), August ($p < 0.01$ via linear regression) and September ($p = 0.27$ via linear regression), while all other months show lower upward trends.

5 Discussion

5.1 Mass balance sensitivity and its climatic drivers

To assess the sensitivity of the mass balance of Shiyi Glacier to climate change, six independent temperature-change scenarios were designed with air temperatures adjusted in 0.5 °C steps from -1.5 to $+1.5$ °C while other variables and model parameters were held constant. Six independent precipitation-change scenarios were also established in the same way by perturbing the precipitation in 10% steps from -30 to $+30\%$. We reran the model with these 12 scenarios as a sensitivity analysis and the results are presented in Fig. 5. The mass balance sensitivity to temperature change (± 1 °C) is ± 0.74 m w.e.a^{-1} °C, which is essentially in agreement with the sensitivity of Parlung No.94 Glacier (Yang et al. 2013), but lower than those of Qiyi Glacier (Wang et al. 2012), Zhadang Glacier (Mölg et al. 2012; Zhu et al. 2018b) and Parlung No. 4 (Zhu et al. 2018b) on the TP. The mass balance sensitivity to precipitation is calculated as ± 0.18 m w.e. for the 10% change, which corresponds to those of Zhadang Glacier (Mölg et al. 2012) and Parlung No.

94 (Yang et al. 2013), but is lower than that of Qiyi Glacier (Wang et al. 2012).

To further explore potential climate-glacier mass balance relationships, temporal climate variation in the glacierized region during the 54 mass balance years was analysed based on the model forcing data. A significant increasing trend was found in annual mean temperature since the 1990s, while the annual total precipitation had high interannual variability without any significant trend. For glacier mass balance, ice/snow ablation is highly related to surface air temperature, which is usually expressed in the form of cumulative positive temperature, with accumulation estimates based mainly on solid precipitation (Braithwaite 1995; Hock 2003). Compared with annual average temperature and total precipitation, we thought that the cumulative positive temperature and solid precipitation during a mass balance year would more directly reflect the interaction between glacier mass balance and local climatic change. Consequently, we analysed the trends in cumulative positive temperature and solid precipitation from 1963/64 to 2016/17. Cumulative positive temperature showed a statistically significant uptrend ($p < 0.01$ via linear regression), especially for the period of 1990/91 to 2016/17. Meanwhile, a slightly increasing trend was found for solid precipitation, without an obvious periodic fluctuation (Fig. 6).

Moreover, a notable increase in the number of cumulative positive temperature day (CPTD) since the 1990s was found. Mean daily temperature increased more notably in 1990/91–2016/17 than in 1963/64–1989/90 (Fig. 7). It can clearly be seen that the number of CPTD increased at a rate of 0.34 d.a^{-1} under the background of climatic warming on the TP, especially after the 1990s, which directly extended the length of the ablation season (May–September). There is high synchronization between the interannual variations
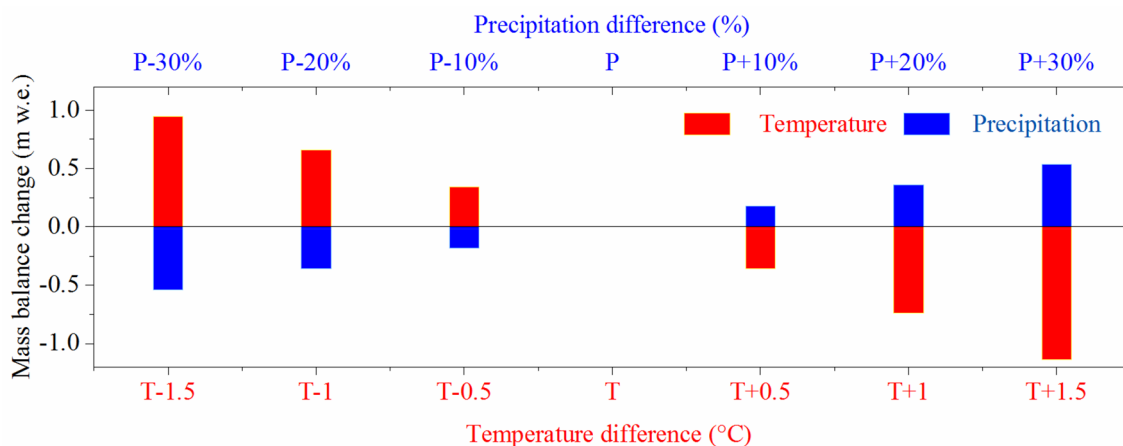

Fig. 5 Mass balance sensitivity of the Shiyi Glacier under various temperature/precipitation-change scenarios. Air temperature was perturbed in 0.5 °C steps and precipitation was perturbed in 10% steps.

Mass balance changes due to precipitation and temperature perturbations are shown in blue and red, respectively
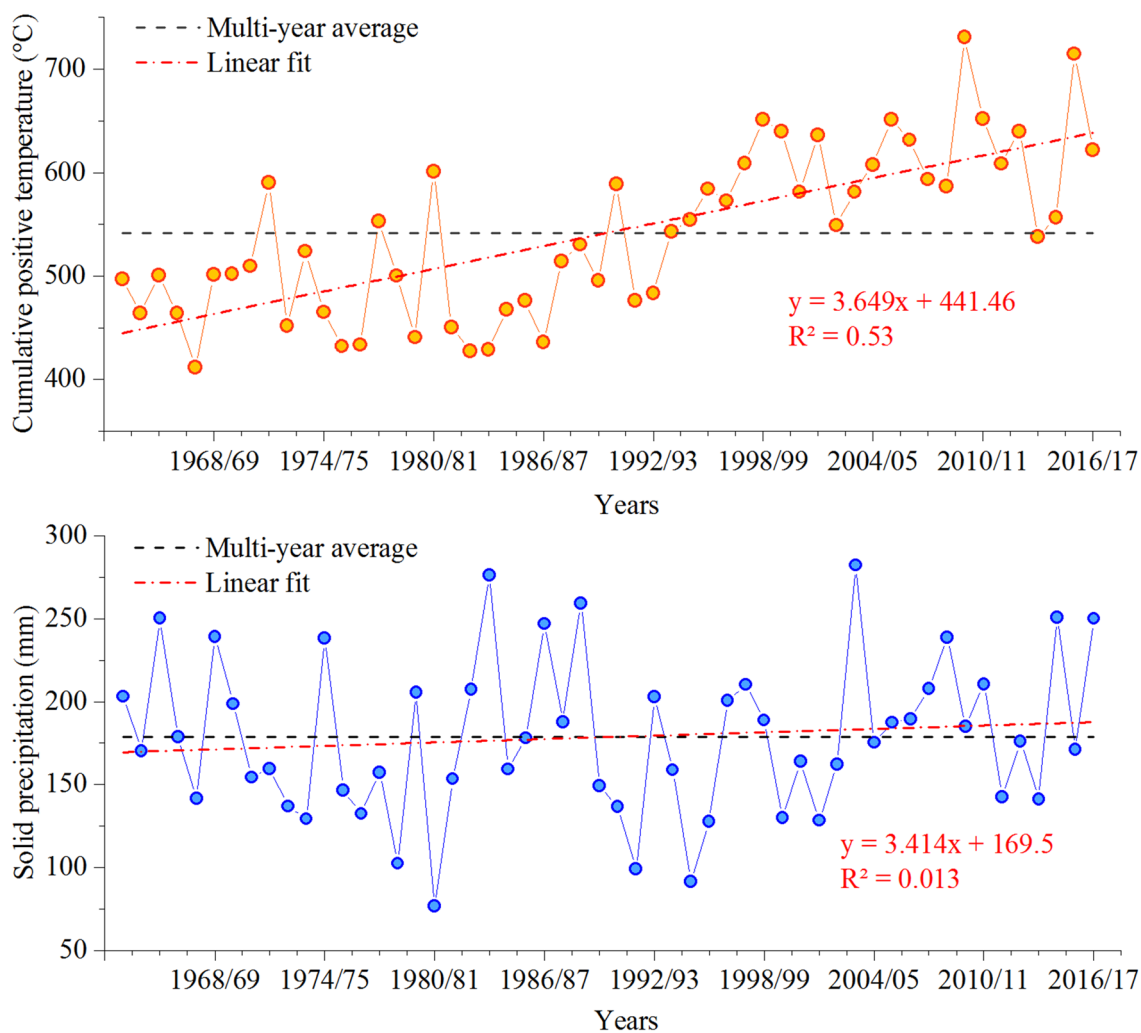
Fig. 6 Variations in cumulative positive temperature and solid precipitation from 1963/64 to 2016/17 based on model forcing data. Solid precipitation was acquired through snow/rain separation by T_p. The dotted line represents multiyear ensemble averages
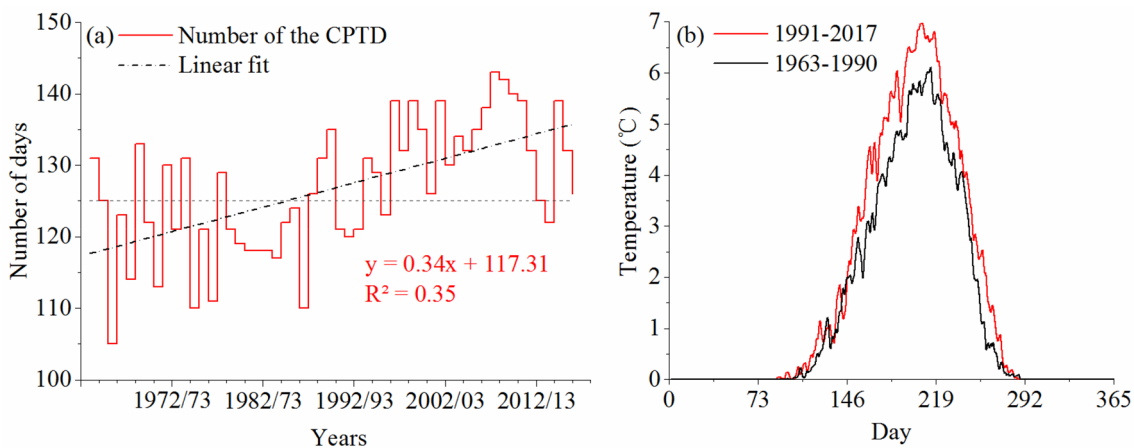
Fig. 7 Variations in the number of the CPTD from 1963/1964 to 2016/2017 (**a**), and mean daily temperatures (> 0 ℃) for two periods (1963–1990 and 1991–2017) (**b**) based on model forcing data. The dotted line indicates multiyear averages

in cumulative positive temperature and reconstructed annual mass balance. Reconstructed annual mass balance correlated well with cumulative positive temperature and solid precipitation, with correlation coefficients of 0.73 ($p < 0.01$) and 0.43 ($p < 0.01$), respectively.

From the monthly perspective, monthly ablation (1990/91–2016/17) was significantly higher than that in phase I (1963/64–1989/90), and a decrease was found in accumulation (solid precipitation) from June to September in phase II, which was affected by a temperature rise on the glacier surface. Mass balance evolution is mainly controlled by the local hydrothermal conditions (covariation of temperature and precipitation), with a negative (positive) mass balance commonly related to a higher (lower) cumulative positive temperature and less (more) solid precipitation. A lower temperature on the glacier surface during the ablation season is favourable to the accumulation, which prevents excessive melting by increasing the surface albedo (Fujita et al. 2010). Additionally, a higher

temperature also partly reduces the amount of solid precipitation, thereby intensifying glacier ablation. According to the field observations and simulations (Fig. S2), ablation and accumulation at Shiyi Glacier are both mainly concentrated in the summer half-year.

5.2 Relationships between large-scale circulations and interannual mass balance changes

Evaluating the possible contribution of large-scale circulation systems to local mass balance can be beneficial in explaining the contemporary variations, palaeo-extents and ice core statistics of glaciers in High Asia (Mölg et al. 2014). Based on periodic changes in annual mass balance at Shiyi Glacier, we explored the potential association between macro-scale atmospheric circulation and glacier mass change. The 300 hPa geopotential height/horizontal wind anomalies (June–September) for the two phases were used to discern shifts in regional circulation patterns

Fig. 8 Composites of the 300 hPa geopotential height and horizontal wind anomalies for June to September for the periods 1963/64–1989/90 (**a**) and 1990/91–2016/17 (**b**). The red dots indicate the location of Shiyi Glacier, white lines denote the borders of continents and the red line shows the boundary of the TP. Data provided by NECP/NCAR
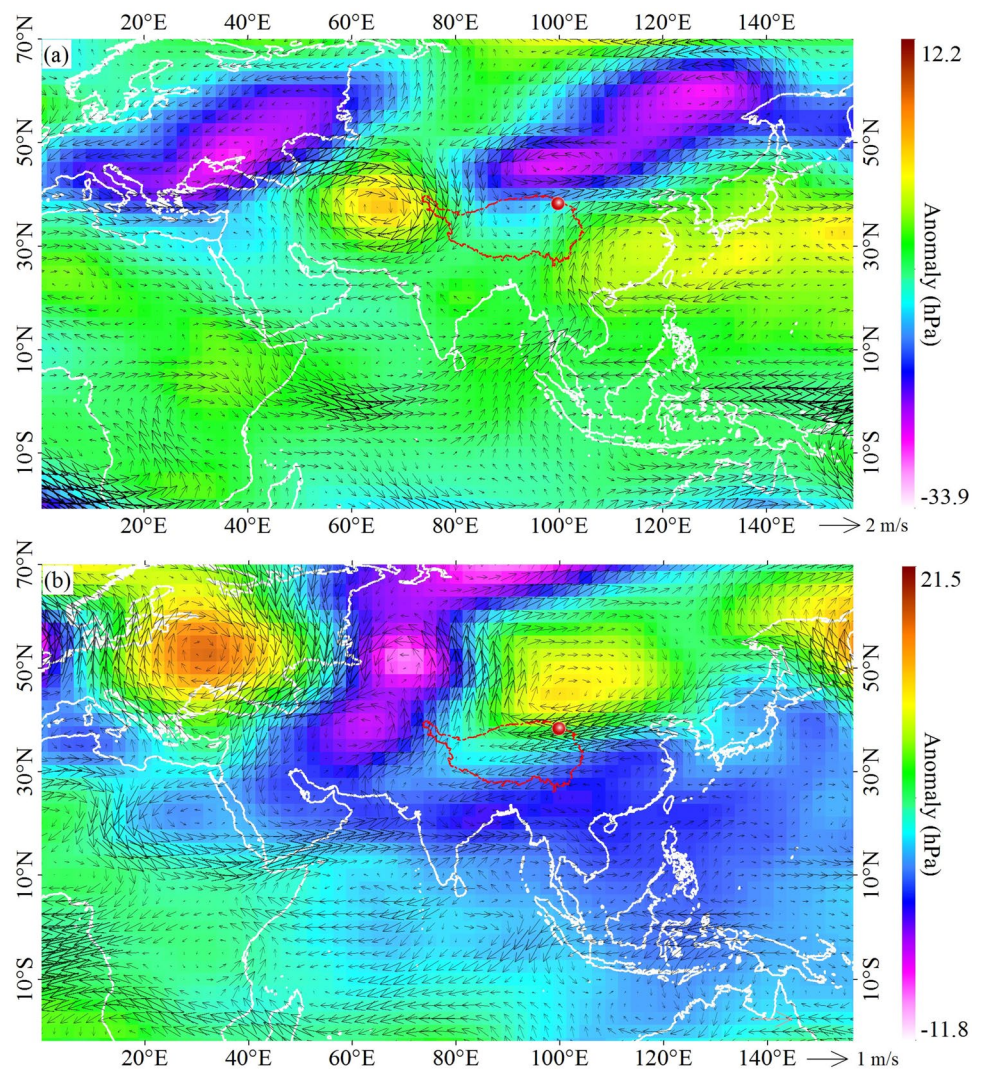
(Fig. 8). For the period 1963/64–1989/1990, when a positive mass balance dominated, the 300 hPa geopotential height (June to September) for the mid-latitude region in the Northern Hemisphere was located significantly higher in Central Asia, northern Pakistan and southeastern China and considerably lower in Southern and Eastern Europe, northern China-Inner Mongolia and eastern Russia. In general, a spatial pattern in geopotential height change (positive–negative-positive) appears to exist in northern hemisphere mid-latitudes. Coupled with changes in geopotential height, cyclonic/anti-cyclonic circulations occur separately in corresponding low/high-pressure centres. The geopotential height changed to the opposite spatial pattern (negative–positive-negative) during the period 1990/91–2016/17, which also led to a shift in horizontal wind direction (cyclonic/anti-cyclonic circulation).

Meanwhile, we found that the glacierized region was associated with a westerly wind anomaly during the period 1963/64–1989/1990 and an easterly wind anomaly during the period 1990/91–2016/17. Anti-cyclonic circulation occurred in northern China-Inner Mongolia and eastern Russia from 1990/91–2016/17 (Fig. 8), which reduced the wind speed in the glacierized region. Interannual fluctuations in zonal wind speed accord well with those of annual mass balance (Fig. 9), with a positive correlation found between them ($r = 0.54$, $p < 0.01$). Hence, it appears that there is a correlation between the mass balance of Shiyi Glacier and large-scale climate dynamics.

Wind speeds correlate well with summer air temperatures in the TP, and wind declines have contributed to TP warming during summer half-years (Yang et al. 2014, 2016). Such wind declines may weaken regional water-vapour exchange between TP and Asian monsoon regions and reduce precipitation; however, warming and accompanying moistening increases local atmospheric instability, which triggers vertical mixing, thicker cloud cover and more precipitation (Yang et al. 2012).

To further explore the teleconnection between macroscale climatic patterns and specific glacier mass balances, we tested the correlation of annual mass balance with major monthly teleconnection indexes during the period 1963/64–2016/17, including the EA, EP-NP, PDO, WP, EA-WR, NAO, PNA and NP. The results show that a significant anticorrelation exists between the July EA index and annual mass balance ($r = -0.47$, $p < 0.01$; Fig. 10). To clarify their specific relationship, the correlations between the July EA index and cumulative positive temperature/solid precipitation were evaluated separately. We found the July EA index to correlate well with the cumulative positive temperature ($r = 0.7$, $p < 0.01$), but it correlated poorly with solid precipitation. The interannual fluctuations in cumulative positive temperature and July EA index are generally consistent (Fig. 10). This kind of strong positive correlation between Europe and eastern China has been reported by Yang et al. (2016). Such a zonal atmospheric teleconnection pattern across mid-latitude Eurasia exerts a notable influence on temperature changes in glacierized regions, thus directly affecting glacier mass turnover processes.
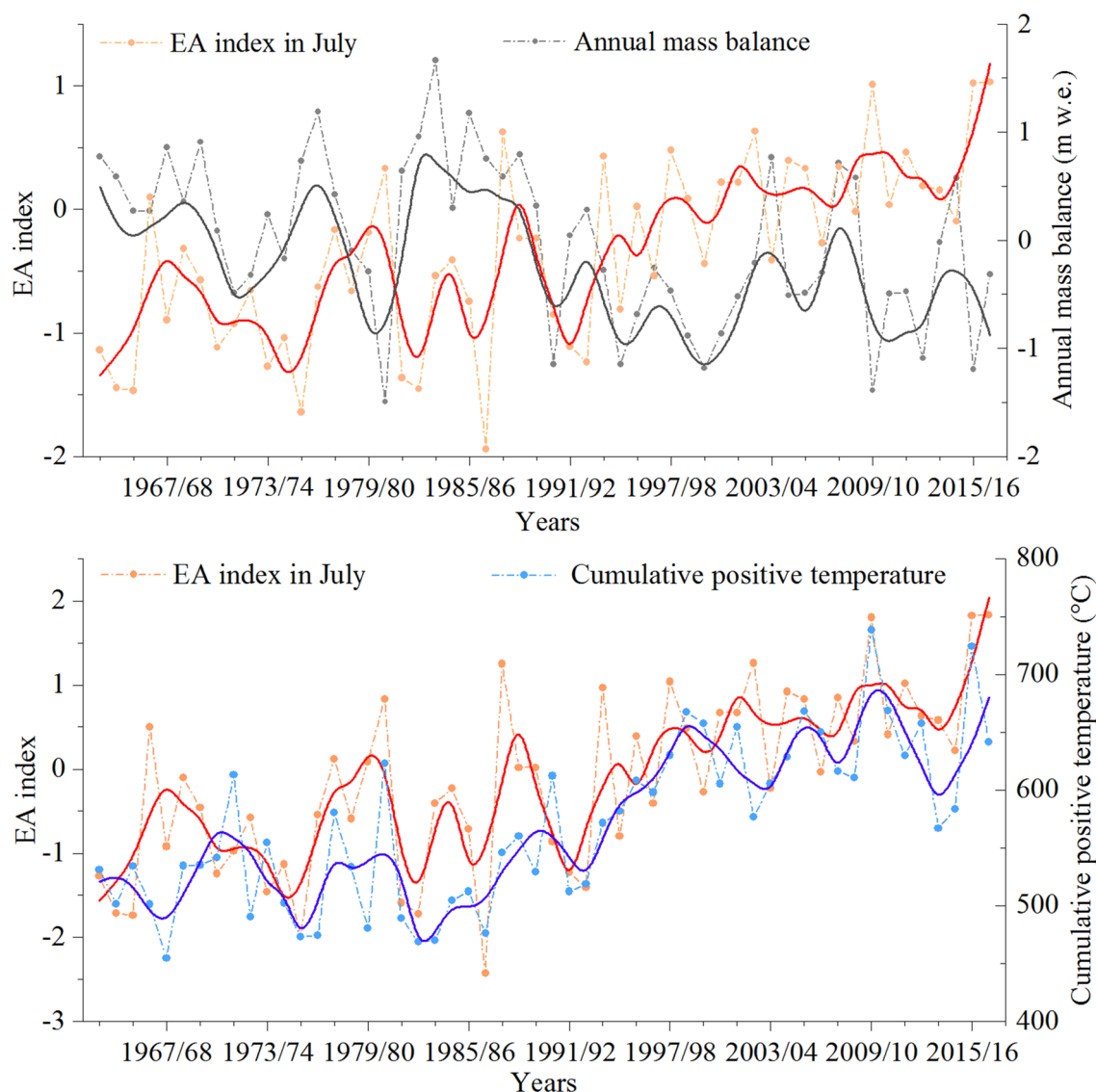
5.3 Comparison with other monitored glaciers on the TP

Although some glacier mass balance data are available for the TP (Yao et al. 2012), long-term data series remain
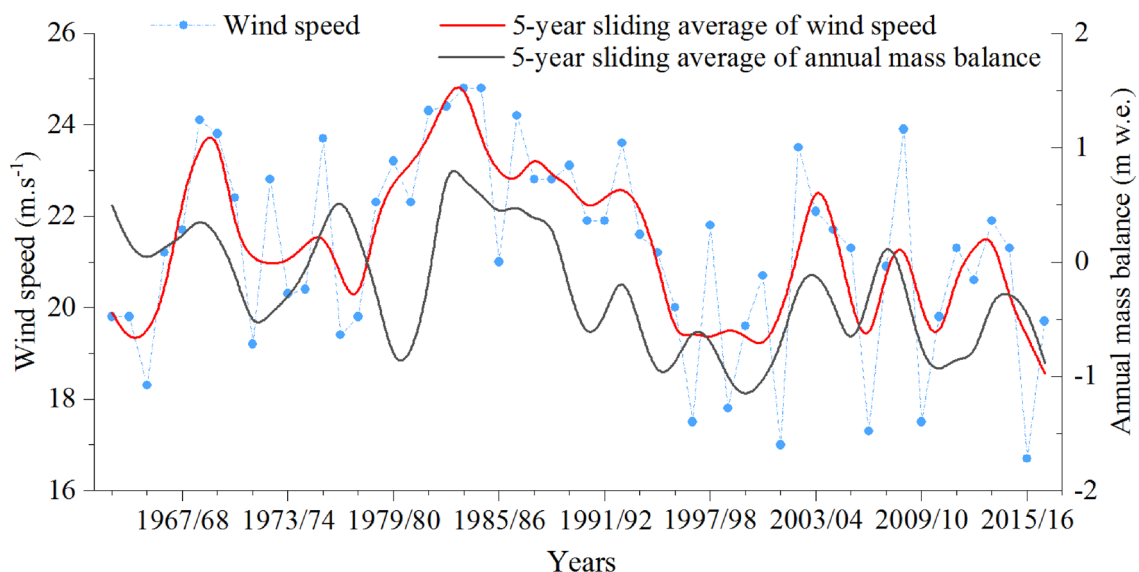
Fig. 9 Time series of zonal wind speeds (June–September) at the 300 hPa geopotential height from 1963/64 to 2016/17

Fig. 10 Comparisons of July EA index vs annual mass balance (above) and vs cumulative positive temperature (below) from 1963/64 to 2016/17. Black, red and blue solid lines indicate the 5-year sliding averages of annual mass balance, July EA index, and cumulative positive temperature, respectively

scarce. To shed further light on spatiotemporal changes in glacier mass across the TP, long-term annual mass balances for six selected glaciers (based on a combination of in-situ and reconstructed data) were compared (Fig. 11). The spatial distribution of the glaciers is relatively uniform and they are located separately in the northeast, southeast, middle, southwest and northwest of the TP. As shown, interannual and periodical variations in annual mass balance for Parlung Glacier No. 94 and Muztag Ata Glacier differ dramatically from those of the other four glaciers. Kangwure Glacier, Shiyi Glacier, Xiaodongkemadi Glacier and Qiyi Glacier have both exhibited an accelerating negative trend in net mass balance since the beginning of the 1990s. However,

Parlung Glacier No. 94 turned increasingly negative until 2002, while Muztag Ata Glacier showed a slight upward trend in positive mass balance. Due to the time series lengths differing between glaciers, we compared their annual values from 1992 to 2010, within which data were available for all glaciers. The results show that annual mass balances from lowest to highest were: Kangwure Glacier, Shiyi Glacier, Parlung No. 94, Qiyi Glacier, Xiaodongkemadi Glacier and Muztag Ata No. 15. This corresponds to the pattern of spatial differences proposed by Yao et al. (2012).

Spatial differences in glacier mass balance change on the TP have been ascribed to differences in local climatic regimes (such as air temperature increases,
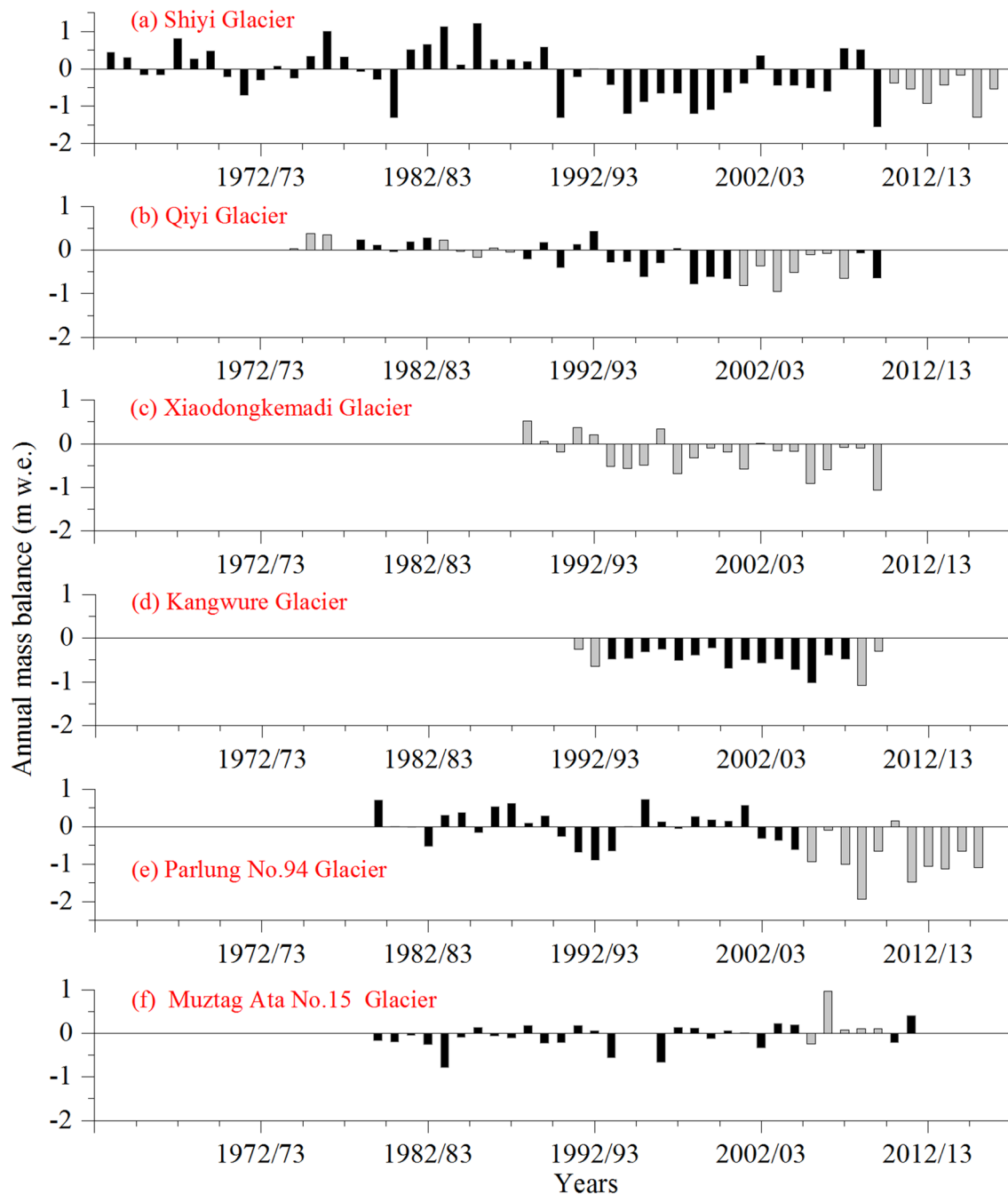
Fig. 11 Comparison of annual mass balances of Shiyi Glacier (SY) and five other glaciers (**a–f**) with available long-term (≥ 19 years) mass balance time series. Mass balance data sources: WGMS (2019) for measured data; Yao et al. (2012) for reconstructed data for Qiyi Glacier (QY), Xiaodongkemdi Glacier (XDKMD) and Kangwure Glacier (KW); Yang et al. (2016) for reconstructed data for Parlung No. 94 (PL); and Zhu et al. (2018a) for reconstructed data for Muztag Ata Glacier (MA). Grey and black bars indicate the measured and reconstructed data, respectively

snowfall-precipitation ratio, energy during the ablation season, precipitation seasonality) and each monitored glacier's size, shape and topographic factors (aspect, slope, altitudinal range) (Yao et al. 2012; Zhu et al. 2018a). Many observations and studies have shown that climatic warming on the TP became significant in the 1960s, with obvious

regional differences (Yang et al. 2019). The most remarkable warming occurred in the northern region (Wang et al. 2018), with obvious warming also occurring in the central and northwestern regions (Liu and Chen 2000). Spatial differences in precipitation are also significant across the TP, especially for the northern and southern plateaus

(Yang et al. 2019). The trends in precipitation variation are negative in the western, eastern, southern and south-eastern regions (Li et al. 2010; Chen et al. 2013; Yang et al. 2014; Gao et al. 2015) but positive in the central and northeastern TP (Wang et al. 2014, 2018). Meanwhile, region-wide snowfall showed an upward trend before the 1980s and then rapid declines for most areas of the TP, especially on the northeastern and eastern plateaus (Deng et al. 2017). Asynchronous climatic change in different glacierized regions would also lead to inconsistent inter-annual fluctuations in glacier mass balance across the TP.

6 Conclusions

In this study, annual mass balances for Shiyi Glacier in the northeast Tibetan Plateau were determined using the gla-ciological method for seven mass balance years. The annual and seasonal mass balances for Shiyi Glacier in the north-east Tibetan Plateau were reconstructed using a temperature-index model of the period 1963/64 to 2016/17. The model was calibrated by in-situ mass balance data and validated by periodic geodetic mass balance data (2000–2012). The reconstructed annual mass balance experienced an over-all downward trend over the 54 mass balance years, with remarkably high mass loss after 1989/90. The pronounced mass loss of Shiyi Glacier since the 1990s can be mainly attributed to cumulative positive temperature increases caused by rising air temperatures and prolongation of the ablation season. For the positive/negative phase of the annual mass balance, an inverse spatial pattern in relation to geopotential height change (low/high-pressure centres) and corresponding conversion of cyclonic/anti-cyclonic cir-culation were present in northern hemisphere mid-latitudes.

We found that the July EA index was highly correlated with the cumulative positive temperature of the glacier-ized region and inversely related to the glacier mass bal-ance. It appears that the mass balance for Shiyi Glacier in July is remotely linked with climate changes in mid-latitude Europe, which exert influences on temperatures in the gla-cierized region and, thus, directly affect glacier mass turno-ver processes. For glacier mass change across the TP, intra-regional discrepancies in climatic change not only determine the magnitude of difference but also cause inconsistent interannual fluctuations. Taken together, the findings of this research strengthen current knowledge of glacier-climate interactions in the Qilian Mountains (northeastern TP) and provide a basis for further research on mass-balance evolu-tion across the TP.

Given the limitations of the temperature index model and parameterisation scheme used in this study, further research that includes geodetic mass-balance measurements and energy-balance studies would be conducive to more accu-rately quantifying the mass budget of Shiyi Glacier. It would also provide a deeper understanding of the contributions of different energy fluxes to the processes involved in mass balance evolution.

References

Azam M, Wagnon P, Ramanathan A, Vincent C, Sharma P, Arnaud Y, Linda A, George J, Pottakkal JG, Chev-allier P, Singh VB, Berth-ier E (2012) From balance to imbalance: a shift in the dynamic behaviour of Chhota Shigri glacier, western Himalaya, India. J Glaciol 58(208):315–324. https://doi.org/10.3189/2012JoG11J123

Azam MF, Wagnon P, Vincent C, Ramanathan A, Linda A, Singh VB (2014) Reconstruction of the annual mass balance of Chhota Shi-gri glacier, Western Himalaya, India, since 1969. Ann Glaciol 55(66):69–80. https://doi.org/10.3189/2014aog66a104

Barandun M, Huss M, Sold L, Farinotti D, Azisov E, Salzmann N, Usubaliev R, Merkushkin A, Hoelzle M (2015) Re-analysis of seasonal mass balance at Abramov glacier 1968–2014. J Glaciol 61(230):1103–1117. https://doi.org/10.3189/2015JoG14J239

Barandun M, Huss M, Usubaliev R, Azisov E, Berthier E, Kaab A, Bolch T, Hoelzle M (2018) Multi-decadal mass balance series of three Kyrgyz glaciers inferred from modelling constrained with repeated snow line observations. Cryosphere 12(6):1899–1919. https://doi.org/10.5194/tc-2017-256-rc1

Bolch T (2012) The state and fate of Himalayan glaciers. Science 336(6079):310–314. https://doi.org/10.1126/sci-ence.1215828

Bonekamp PNJ, de Kok RJ, Collier E, Immerzeel WW (2019) Con-trasting meteorological drivers of the glacier mass balance between the Karakoram and Central Himalaya. Front Earth Sci 7:107. https://doi.org/10.3389/feart.2019.00107

Braithwaite RJ (1995) Positive degree-day factors for ablation on the Greenland ice-sheet studied by energy-balance modeling. J Gla-ciol 41(137):153–160. https://doi.org/10.1017/s00221430000178 46

Braithwaite RJ, Zhang Y (2000) Sensitivity of mass balance of five Swiss glaciers to temperature changes assessed by tun-ing a degree-day model. J Glaciol 46(152):7–14. https://doi.org/10.3189/172756500781833511

Brun F, Berthier E, Wagnon P, Kääb A, Désirée T (2017) A spatially resolved estimate of high mountain asia glacier mass balances from 2000 to 2016. Nat Geosci 10(9):668–673. https://doi.org/10.1038/ngeo2999

Brun F, Wagnon P, Berthier E, Jomelli V, Maharjan SB, Shrestha F, Kraaijenbrink PDA (2019) Heterogeneous influence of glacier

morphology on the mass balance variability in High Mountain Asia. J Geophys Res Earth 124(6):1331–1345. https://doi.org/10.1029/2018jf004838

Chen H et al (2013) The impacts of climate change and human activities on biogeochemical cycles on the Qinghai Tibetan Plateau. Glob Change Biol 19(10):2940–2955. https://doi.org/10.1111/gcb.12277

Chen RS, Song YX, Kang ES, Han CT, Liu JF, Yang Y, Qing WW, Liu ZW (2014) A cryosphere hydrology observation system in a small alpine watershed in the Qilian Mountains of China and its meteorological gradient. Arct Antarct Alp Res 46(2):505–523. https://doi.org/10.1657/1938-4246-46.2.505

Chen R, Liu J, Kang E, Yang Y, Han C, Liu Z, Song Y, Qing W, Zhu P (2015) Precipitation measurement intercomparison in the Qilian Mountains, north-eastern Tibetan Plateau. Cryosphere 9(5):1995–2008. https://doi.org/10.5194/tc-9-1995-2015

Cogley JG (2009) Geodetic and direct mass-balance measurements: comparison and joint analysis. Ann Glaciol 50(50):96–100. https://doi.org/10.3189/172756409787769744

De Kok RJ, Tuinenburg OA, Bonekamp PNJ, Immerzeel WW (2018) Irrigation as a potential driver for anomalous glacier behavior in High Mountain Asia. Geophys Res Lett 45(4):2047–2054. https://doi.org/10.1002/2017GL076158

Deng HJ, Pepin NC, Chen YN (2017) Changes of snowfall under warming in the Tibetan Plateau. J Geophys Res Atmos 122(14):7323–7341. https://doi.org/10.1002/2017jd026524

Fang XY, Li ZQ, Bernd W, Gao S, Chen RS (2015) Physical energy-balance and statistical glacier melting models comparison and testing for Shiyi Glacier, Heihe River Basin, Qilian Mountains, China. J Glaciol Geocryol 37(2):336–350 (**In Chinese**)

Farinotti D, Immerzeel WW, de Kok RJ, Quincey DJ, Dehecq A (2020) Manifestations and mechanisms of the Karakoram glacier anomaly. Nat Geosci 13(1):8–16. https://doi.org/10.1038/s41561-019-0513-5

Fujita K, Ohta T, Ageta Y (2010) Characteristics and climatic sensitivities of runoff from a cold-type glacier on the Tibetan Plateau. Hydrol Process 21(21):2882–2891. https://doi.org/10.1002/hyp.6505

Fujita K, Nuimura T (2011) Spatially heterogeneous wastage of Himalayan glaciers. Proc National Acad Sci United States Am 108(34):14011–14014. https://doi.org/10.1073/pnas.1106242108

Fujita K, Takeuchi N, Nikitin SA, Surazakov AB, Okamoto S, Aizen VB, Kubota J (2011) Favorable climatic regime for maintaining the present-day geometry of the Gregoriev Glacier, Inner Tien Shan. Cryosphere 5(3):539–549. https://doi.org/10.5194/tc-5-539-2011

Gao YH, Li X, Leung LR, Chen DL, Xu JW (2015) Aridity changes in the Tibetan Plateau in a warming climate. Environ Res Lett 10(3):034013. https://doi.org/10.1088/1748-9326/10/3/034013

Gardelle J, Berthier E, Arnaud Y, Kaab A (2013) Region-wide glacier mass balances over the Pamir–Karakoram–Himalaya during 1999–2011. Cryosphere 7(6):1885–1886. https://doi.org/10.5194/tc-7-1263-2013

Hock R (2003) Temperature index melt modelling in mountain areas. J Hydrol 282(1–4):104–115. https://doi.org/10.1016/s0022-1694(03)00257-9

Huss M, Bauder A, Funk M, Hock R (2008) Determination of the seasonal mass balance of four Alpine glaciers since 1865. J Geophys Res Earth 113(F1):F01015. https://doi.org/10.1029/2007jf000803

Immerzeel WW, Van Beek LP, Bierkens MF (2010) Climate change will affect the Asian water towers. Science 328(5984):1382–1385. https://doi.org/10.1126/science.1183188

Kääb A, Treichler D, Nuth C, Berthier E (2015) Brief Communication: contending estimates of 2003–2008 glacier mass balance over the Pamir–Karakoram–Himalaya. Cryosphere 9(2):557–564. https://doi.org/10.5194/tc-9-557-2015

Kaser G, Cogley JG, Dyurgerov MB, Meier MF, Ohmura A (2006) Mass balance of glaciers and ice caps: consensus estimates for 1961–2004. Geophys Res Lett 33(19):L19501. https://doi.org/10.1029/2006gl027511

Kenzhebaev R, Barandun M, Kronenberg M, Chen YN, Usubaliev R, Hoelzle M (2017) Mass balance observations and reconstruction for Batysh Sook Glacier, Tien Shan, from 2004 to 2016. Cold Reg Sci Technol 135:76–89. https://doi.org/10.1016/j.coldregions.2016.12.007

Kronenberg M, Barandun M, Hoelzle M, Huss M, Farinotti D, Azisov E, Usubaliev R, Gafurov A, Petrakov D, Kääb A (2016) Mass-balance reconstruction for Glacier No. 354, Tien Shan, from 2003 to 2014. Ann Glaciol 57(71):92–102. https://doi.org/10.3189/2016AoG71A032

Kumar P, Saharwardi MS, Banerjee A, Azam MFA, Dubey AK, Murtugudde R (2019) Snowfall variability dictates glacier mass balance variability in Himalaya–Karakoram. Sci Rep 9:18192. https://doi.org/10.1038/s41598-019-54553-9

Li L, Yang S, Wang ZY, Zhu XD, Tang HY (2010) Evidence of warming and wetting climate over the Qinghai Tibet Plateau. Arct Antarct Alp Res 42(4):449–457. https://doi.org/10.1657/1938-4246-42.4.449

Liang L, Cuo L, Liu Q (2019) Mass balance variation and associative climate drivers for the Dongkemadi Glacier in the central Tibetan Plateau. J Geophys Res Atmos 124(20):10814–10825. https://doi.org/10.1029/2019JD030615

Liu XD, Chen BD (2000) Climatic warming in the Tibetan Plateau during recent decades. Int J Climatol 20(14):1729–1742

Liu J, Chen R (2016) Discriminating types of precipitation in Qilian Mountains, Tibetan Plateau. J Hydrol Reg Stud 5(C):20–32. https://doi.org/10.1016/j.ejrh.2015.11.013

Liu Q, Liu SY (2016) Response of glacier mass balance to climate change in the Tianshan Mountains during the second half of the twentieth century. Clim Dyn 46(1–2):303–316. https://doi.org/10.1007/s00382-015-2585-2

Liu JF, Chen RS, Han CT, Qing WW (2016) Two-year comparative study of snow cover dynamics and its impact factors on glacier surface. Environ Earth Sci 75(3):197. https://doi.org/10.1007/s12665-015-5075-2

Machguth H, Haeberli W, Paul F (2012) Mass-balance parameters derived from a synthetic network of mass balance glaciers. J Glaciol 58(211):965–979. https://doi.org/10.3189/2012jog11j223

Marzeion B, Cogley JG, Richter K, Parkes D (2014) Attribution of global glacier mass loss to anthropogenic and natural causes. Science 345(6199):919–921. https://doi.org/10.1126/science.1254702

Mölg T, Maussion F, Yang W, Scherer D (2012) The footprint of Asian monsoon dynamics in the mass and energy balance of a Tibetan glacier. Cryosphere 6(6):1445–1461. https://doi.org/10.5194/tc-6-1445-2012

Mölg T, Maussion F, Scherer D (2014) Mid-latitude westerlies as a driver of glacier variability in monsoonal High Asia. Nat Clim Change 4(1):68–73. https://doi.org/10.1038/nclimate2055

Neckel N, Kropacek J, Bolch T, Hochschild V (2014) Glacier mass changes on the Tibetan Plateau 2003–2009 derived from ICESat laser altimetry measurements. Environ Res Lett 9(1):014009. https://doi.org/10.1088/1748-9326/9/1/014009

Oerlemans J (1994) Quantifying global warming from the retreat of glaciers. Science 264(5156):243–245. https://doi.org/10.1126/science.264.5156.243

Paterson WSB (1994) The physics of glaciers, 3rd edn. Pergamon, New York, pp 26–52

Paul F et al (2013) On the accuracy of glacier outlines derived from remote-sensing data. Ann Glaciol 54(63):171–182. https://doi.org/10.3189/2013AoG63A296

Pellicciotti F, Brock B, Strasser U, Burlando P, Funk M, Corripio J (2005) An enhanced temperature-index glacier melt model including the shortwave radiation balance: development and testing for Haut Glacier d'Arolla, Switzerland. J Glaciol 51(175):573–587. https://doi.org/10.3189/172756505781829124

Reveillet M, Vincent C, Six D, Rabatel A (2017) Which empirical model is best suited to simulate glacier mass balances? J Glaciol 63(237):39–54. https://doi.org/10.1017/jog.2016.110

Shean DE, Bhushan S, Montesano P, Rounce DR, Arendt A, Osmanoglu B (2020) A systematic, regional assessment of high mountain asia glacier mass balance. Front Earth Sci 7:363. https://doi.org/10.3389/feart.2019.00363

Shi YF (2008) Concise glacier inventory of China. Shanghai Popular Science Press, Shanghai, pp 36–37

Sicart JE, Hock R, Six D (2008) Glacier melt, air temperature, and energy balance in different climates: the Bolivian Tropics, the French Alps, and northern Sweden. J Geophys Res Atmos 113:D24113. https://doi.org/10.1029/2008JD010406

Thibert E, Blanc R, Vincent C, Eckert N (2008) Glaciological and volumetric mass-balance measurements: error analysis over 51 years for Glacier de Sarennes, French Alps. J Glaciol 54(186):522–532. https://doi.org/10.3189/002214308785837093

Vincent C (2002) Influence of climate change over the 20th Century on four French glacier mass balances. J Geophys Res Atmos 107(D19):ACL 4-1-ACL 4-12. https://doi.org/10.1029/2001jd000832

Wang NL, He JQ, Pu JC, Jiang X, Jing ZF (2010) Variations in equilibrium line altitude of the Qiyi Glacier, Qilian Mountains, over the past 50 years. Chin Sci Bull 55(33):3810–3817. https://doi.org/10.1007/s11434-010-4167-3

Wang S, Pu JC, Wang NL (2012) Study on mass balance and sensitivity to climate change in summer on the Qiyi Glacier, Qilian Mountains. Sci Cold Arid Reg 4(4):281–287. https://doi.org/10.3724/sp.j.1226.2012.00281

Wang XJ, Yang MX, Liang XW, Pang GJ, Wan GN, Chen XL, Luo XQ (2014) The dramatic climate warming in the Qaidam Basin, northeastern Tibetan Plateau, during 1961–2010. Int J Climatol 34(5):1524–1537. https://doi.org/10.1002/joc.3781

Wang XJ, Pang GJ, Yang MX (2018) Precipitation over the Tibetan Plateau during recent decades: a review based on observations and simulations. Int J Climatol 38(3):1116–1131. https://doi.org/10.1002/joc.5246

WGMS (2019) Fluctuations of Glaciers Database. World Glacier Monitoring Service, Zurich, Switzerland. https://doi.org/10.5904/wgms-fog-2019-12

Xu CH, Li ZQ, Wang FT, Ha L, Yagoub YE, Jin S (2019) Recent geodetic mass balance and extent changes of very small glaciers in the Hulugou Basin, Central Qilian Mountains, China. J Earth Syst Sci 128(3):47. https://doi.org/10.1007/s12040-019-1067-z

Yamamoto R, Iwashima T, Sanga NK, Hoshiai M (1986) An analysis of climatic jump. J Meteor Soc Jpn 64(2):273–281

Yang K, Ding BH, Qin J, Tang WJ, Lu N, Lin CG (2012) Can aerosol loading explain the solar dimming over the Tibetan Plateau?

Geophys Res Lett 39:L20710. https://doi.org/10.1029/2012GL053733

Yang W, Yao TD, Guo XF, Zhu ML, Li SH, Kattel DB (2013) Mass balance of a maritime glacier on the southeast Tibetan Plateau and its climatic sensitivity. J Geophys Res Atmos 118(17):9579–9594. https://doi.org/10.1002/jgrd.50760

Yang K, Wu H, Qin J, Lin CG, Tang WJ, Chen YY (2014) Recent climate changes over the Tibetan Plateau and their impacts on energy and water cycle: a review. Glob Planet Change 112:79–91. https://doi.org/10.1016/j.gloplacha.2013.12.001

Yang W, Guo XF, Yao TD, Zhu ML, Wang YJ (2016) Recent accelerating mass loss of southeast Tibetan glaciers and the relationship with changes in macroscale atmospheric circulations. Clim Dyn 47(3–4):805–815. https://doi.org/10.1007/s00382-015-2872-y

Yang MX, Wang XJ, Pang GJ, Wang GN, Liu ZC (2019) The Tibetan Plateau cryosphere: observations and model simulations for current status and recent changes. Earth Sci Rev 190:353–369. https://doi.org/10.1016/j.earscirev.2018.12.018

Yao TD et al (2012) Different glacier status with atmospheric circulations in Tibetan Plateau and surroundings. Nat Clim Change 2(9):663–667. https://doi.org/10.1038/nclimate1580

Zemp M, Hoelzle M, Haeberli W (2009) Six decades of glacier mass-balance observations: a review of the world wide monitoring network. Ann Glaciol 50(50):101–111. https://doi.org/10.3189/172756409787769591

Zemp M et al (2013) Reanalysing glacier mass balance measurement series. Cryosphere 7(4):1227–1245. https://doi.org/10.5194/tc-7-1227-2013

Zemp M et al (2019) Global glacier mass changes and their contributions to sea-level rise from 1961 to 2016. Nature 568(7752):382–386. https://doi.org/10.1038/s41586-019-1071-0

Zhang Y, Liu SY, Ding YJ (2006) Observed degree-day factors and their spatial variation on glaciers in western China. Ann Glaciol 43:301–306. https://doi.org/10.3189/172756406781811952

Zhang H, Li ZQ, Zhou P, Zhu XF, Wang L (2018) Mass-balance observations and reconstruction for Haxilegen Glacier No. 51, eastern Tien Shan, from 1999 to 2015. J Glaciol 64(247):689–699. https://doi.org/10.1017/jog.2018.58

Zhu ML, Yao TD, Yang W, Xu BQ, Wu GJ, Wang XJ (2018b) Differences in mass balance behaviour for three glaciers from different climatic regions on the Tibetan Plateau. Clim Dyn 50(9–10):3457–3484. https://doi.org/10.1007/s00382-017-3817-4

Zhu ML, Yao TD, Yang W, Xu BQ, Wu GJ, Wang XJ, Xie Y (2018a) Reconstruction of the mass balance of Muztag Ata No. 15 glacier, eastern Pamir, and its climatic drivers. J Glaciol 64(244):259–274. https://doi.org/10.1017/jog.2018.16